Understanding Comparisons between WHDG and ASW Single Hard Quenching Weights

B. Cole, W. A. Horowitz

July 2, 2009

1 Introduction

This note describes an analysis of the differences found by Van Leuwen as part of the TECHQM Brick studies between the ASW Single-Hard quenching weights and results from WHDG. A list of the known differences and differences (re)discovered as part of this analysis is:

- WHDG uses thermal masses for quarks and gluons. ASW does not.
- WHDG assumes a different position dependence for the in-medium scattering centers in the evaluation of the phase factor in the leading term in the opacity expansion. ASW quenching weights are evaluated for a uniform distribution of scattering positions; WHDG is by default evaluated with exponential distribution (see below).
- In the opacity expansion $L/\lambda \equiv n_0 L$ is a parameter of the calculation. The ASW single-hard quenching weight code uses fixes $L/\lambda = 1$; in WHDG, λ is determined by medium properties and the path length L is allowed to fluctuate. For the purposes of comparison, the TECHQM brick analyzed in this note has fixed $L = 2$ fm and $T = 485$ MeV (leading to fixed $\mu \simeq 0.94$ GeV and $\lambda \simeq 0.62$ fm for fixed $\alpha_s = 0.3$).
- WHDG and ASW use a different cut-off on the $k_\perp$ integration of the radiated gluon. ASW uses $k_{\rm max} = \omega$ where ω is the gluon energy. WHDG by default uses $k_{\rm max} = 2x(1-x)E_{jet}$ where $x = k^+/E^+$.
- WHDG and ASW use different upper limits on the q integration. ASW uses $q^{max} = \infty$; WHDG uses $q^{max} = \sqrt{3\mu E_{jet}}$.
- ASW takes $\alpha_s = 1/3$; most published WHDG results use $\alpha_s = 0.3$.

The purpose of this note is to illustrate the impact of these differences in the implementation of the leading order contribution to the opacity expansion.

In the remainder of this note we describe in detail the basis of the leading-order in opacity calculations from ASW and WHDG and show explicitly how they are similar and where they differ analytically. We then show that when WHDG is modified to include the same limits and assumptions as ASW, it reproduces the results of the ASW-SH quenching weights code. We then evolve the limits/assumptions of WHDG back to their original form and show how the calculations change and how differences with ASW-SH evolve step-by-step. We find that the most important differences between the ASW-SH quenching weights code and WHDG arise from

1. The explicit choice in the ASW-SH quenching weights code of $L/\lambda = 1$.
2. The difference in the limit of integration over the transverse momentum of the gluon, $k_{\max}$.
3. The inclusion of the gluon mass in the WHDG formalism.

These points are discussed in more detail in Section 6

2 Comparison of ASW and WHDG opacity expansion formulae

One may derive the radiative energy loss formulas used in WHDG [1] and the ASW-SH quenching weights [2], as well as their intermediate steps, starting from the DGLV results [3]. DGLV is an extension of the GLV [4–6] opacity expansion for the single inclusive distribution of radiated gluons to include the mass effects of both the parent parton and the radiated gluon. Both the radiative piece of WHDG and the ASW-SH quenching weights use only the energy loss from the first order in opacity; this is justified numerically by the $\lesssim 30\%$ effect of including higher order in opacity terms [7, 8].

We start with the DGLV first order in opacity result for the single inclusive distribution of massive radiated gluons from a massive parent parton, derived from Eq. (83) of [3]:

$$x\frac{dN_g}{dx} = \frac{C_R\alpha_s}{\pi}\frac{L}{\lambda}\int\frac{d^2\mathbf{q}}{\pi}\frac{\mu^2}{\left(\mathbf{q}^2+\mu^2\right)^2}\int\frac{2d^2\mathbf{k}}{\pi}\frac{\mathbf{k}\cdot\mathbf{q}(\mathbf{k}-\mathbf{q})^2-\beta^2\mathbf{q}\cdot(\mathbf{k}-\mathbf{q})}{\left[(\mathbf{k}-\mathbf{q})^2+\beta^2\right]^2\left(\mathbf{k}^2+\beta^2\right)}$$
$$\times\int dz\left[1-\cos\left(\frac{(\mathbf{k}-\mathbf{q})^2+\beta^2}{2Ex}z\right)\right]\rho(z), \tag{1}$$

where C_R is the color factor appropriate for the parent parton, β is the modification due to the mass of the parent parton M and the radiated gluon m_g ($\beta = 0$ for $M = m_g = 0$) and will be discussed further below, and $\rho(z)$ is a function normalized to 1 that describes the distribution in the longitudinal direction z of the medium particle (center) that is scattered off of. Note that E actually denotes the momentum of the jet, an irrelevant difference for light partons but not so inconsequential for heavy quark jets. $\mathbf{q}$ is the momentum transfer between the parent parton and the in-medium scattering center; $\mathbf{k}$ is the momentum carried off by the radiated gluon. See Fig. 1 for a picture illustrating the notation used here. x is the fraction of the jet plus momentum carried away by the radiation; denoting light-cone 4-vectors with $[,]$, the momentum of a radiated massless gluon is

$$k = [k^+, k^-, k_\perp] = [xE^+, \mathbf{k}^2/(xE^+), \mathbf{k}]. \tag{2}$$

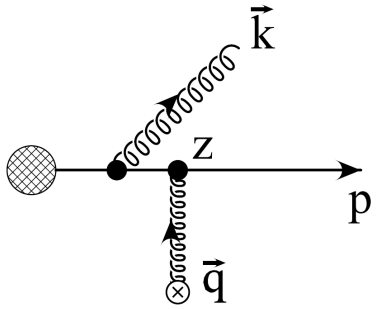

Figure 1: One of the diagrams contributing to the first order in opacity matrix element. $\mathbf{q}$ is the momentum transfer between the parent parton and the in-medium scattering center. $\mathbf{k}$ is the momentum carried off by the radiated gluon. z is the distance from the hard production vertex of the parent parton and the scattering center. Figure adapted from [3].

Two functions of z, both with average values $\bar{z} = L/2$, are commonly used for ρ:

$$\rho_{\text{theta}}(z) = \frac{1}{L}\theta(L - z) \tag{3}$$

$$\rho_{\text{exp}}(z) = \frac{2}{L}\exp\left(-\frac{2z}{L}\right), \tag{4}$$

where we implicitly assume both distributions are multiplied by a $\theta(z)$.

Integrating over the exponential distribution, Eq. (4), as well as over the angular parts of the $\mathbf{k}$ and $\mathbf{q}$ integrals (note that one temporarily assumes

$q_{\max} = \infty$ in order to shift integration variables $\mathbf{q} \to \mathbf{q} - \mathbf{k}$ and analytically perform two integrals; for more details see [3]), the complete WHDG expression for the inclusive gluon spectrum to leading order in the opacity expansion is

$$x\frac{dN_g}{dx} = \frac{C_R\alpha_s}{\pi}\frac{L}{\lambda}\int_0^{q^2_{\max}} \frac{2q^2\mu^2 dq^2}{\left(4xE\hbar c/L\right)^2 + \left(q^2+\beta^2\right)^2} \times \int_0^{k^2_{\max}} \frac{dk^2}{k^2+\beta^2}\frac{k^2\left(k^2-q^2+\mu^2\right) - \beta^2\left(k^2-q^2-\mu^2\right)}{\left((k-q)^2+\mu^2\right)^{3/2}\left((k+q)^2+\mu^2\right)^{3/2}}, \tag{5}$$

where $\beta = x^2M^2 + (1-x)m_g^2$. WHDG restores the $(1-x)$ coefficient to m_g in β dropped in [3] (consistent with the small x approximation), but does not restore any possible overall $(1-x)$ normalization factors [9]. $m_g = \mu/\sqrt{2}$ for the gluon mass, and $M = \mu/2$ for the mass of a parent high-p_T quark; these values were found to be good approximations to the results when using the full HTL propagators [10]. WHDG takes $q_{\max} = \sqrt{3\mu E}$ and $k_{\max} = 2x(1-x)E$; these integration cutoffs will discussed further below. The k integration in Eq. (5) may be performed analytically, but the result is both unwieldy and uninformative.

In the $\beta \to 0$ limit of zero quark and gluon mass, the k integration in Eq. (5) can be performed analytically yielding an expression for the single gluon x distribution

$$x\frac{dN_g}{dx} = \frac{4C_R\alpha_s}{\pi}\frac{L}{\lambda}\int_0^{q_{\max}} dq\frac{\mu^2}{q}\left(\frac{\left(q^2L/2xE\right)^2}{4+\left(q^2L/2xE\right)^2}\right) \times \left(\frac{1}{q^2+\mu^2} - \frac{1}{\sqrt{(q^2-k^2_{max})^2 + 2(q^2+k^2_{max})\mu^2+\mu^4}}\right). \tag{6}$$

The dependence of the spectrum on dimensionful scales can be made more explicit by re-arranging Eq. (6) to

$$x\frac{dN_g}{dx} = \frac{4C_R\alpha_s}{\pi}\frac{L}{\lambda}\int_0^{q_{\max}} \frac{dq}{q}\left[\frac{(q/q_p)^4}{4+(q/q_p)^4}\right] \times \left(\frac{1}{1+\frac{q^2}{\mu^2}} - \frac{1}{\sqrt{\frac{(q^2-k^2_{max})^2}{\mu^4} + 2\frac{(q^2+k^2_{max})}{\mu^2}+1}}\right). \tag{7}$$

where $q_p \equiv \sqrt{2\omega/L}$ is a factor that primarily controls the q-evolution of the "phase" term in the integrand, the term in square brackets that comes from the integral over $\rho(z)$.

The ASW-SH quenching weights [2] are based on the opacity expansion formalism of [11], which reduces to the BDMPS-Z result [12–15] in an infinitely thick medium. (We note that [16] extended [11] to include the effects of a massive parent parton.) Taking the massless limit ($\beta \to 0$) of Eq. (1) and integrating over the θ function distribution, Eq. (3), one arrives at the single inclusive gluon energy distribution implemented in the ASW-SH quenching weights, Eq. (B. 10) of [2]:

$$\omega\frac{dI}{d\omega} = \frac{4\alpha_s C_R}{\pi}(n_0 L)\gamma \int_0^\infty \tilde{q}d\tilde{q}\left[\frac{\tilde{q}^2 - \sin\tilde{q}^2}{\tilde{q}^4}\right] \times \left(\frac{1}{\gamma+\tilde{q}^2} - \frac{1}{\sqrt{(\kappa^2+\tilde{q}^2+\gamma^2)^2 - 4\kappa^2\tilde{q}^2}}\right), \tag{8}$$

where $\gamma = \tilde{\omega}_c/\omega$, $\tilde{\omega}_c = \frac{1}{2}\mu^2 L$, and $\kappa = \sqrt{\omega L/2}$. The factor $n_0 L$ is equivalent to L/λ. In this expression, $\tilde{q}$ and $k_{\rm max}$ have been cast into dimensionless form by factoring out a constant with energy units

$$q = \tilde{q}\sqrt{2\omega/L}, \qquad k_{\rm max} = \kappa\sqrt{2\omega/L}. \tag{9}$$

Implicit in the first expression for κ given above is the choice in the ASW calculations, $k_{\rm max} = \omega$ where ω is the gluon energy. To compare explicitly the ASW radiation spectrum to the WHDG spectrum given above, we return both q and $k_{\rm max}$ to their dimensionful form by inverting the relations in Eq. (9). The spectrum can then be cast into a form similar to that of Eq. (7):

$$\omega\frac{dI}{d\omega} \equiv x\frac{dN_g}{dx} = \frac{4C_R\alpha_s}{\pi}\frac{L}{\lambda}\int_0^{q_{\rm max}}\frac{dq}{q}\left[1 - \frac{\sin\left((q/q_p)^2\right)}{(q/q_P)^2}\right] \times \left(\frac{1}{1+\frac{q^2}{\mu^2}} - \frac{1}{\sqrt{\frac{(q^2-k_{max}^2)^2}{\mu^4} + 2\frac{(q^2+k_{max}^2)}{\mu^2} + 1}}\right). \tag{10}$$

This result is identical in form to the WHDG result except for the term in square brackets which differs from the WHDG form in Eq. (7) due to the different choice for $\rho(z)$. However, we caution that in converting $\omega dI/d\omega$ to dN_g/dx we assumed $\omega = xE$, as is done in [11]. On the other hand recall from Eq. (2) that x in the DGLV formalism is used to specify the fraction of jet plus momentum taken away by the radiated gluon. So while the x distributions in the ASW and WHDG formalisms are identical in form modulo the difference in the phase factor, they actually represent the distribution of different, though related, quantities. This difference has important consequences for the choice of $k_{\rm max}$, as discussed further below.

It is interesting to note that of the two dimensionful parameters one would expect the q-integrand to depend on, the Debye screening μ and the formation time $\tau_{\rm form} = \omega/\mathbf{k}^2$, only the first appears. Rather the shifting of the $\mathbf{q}$ integral used in deriving both Eq. (5) and Eq. (8) results in $q_p \equiv \sqrt{2\omega/L}$ being the second dimensional parameter affecting the dN_g/dx distribution. It is also worth observing that both ASW and WHDG expressions for dN_g/dx to leading order in opacity depend linearly on L/λ. Since $\lambda = 1/\rho\sigma$, there is a factor of the in-medium jet scattering cross-section which implicitly contains two additional powers of α_s.

The single-gluon spectrum depends not only on the input matrix element, which (due to the small $x \ll 1$ limit in which it was derived) knows nothing of the kinematics, but also on the permitted phase space. This is implemented in the upper limits of the k and q integrals in Eq. (5) and Eq. (8). WHDG sets $q_{\rm max} = \sqrt{3\mu E}$ because this is the maximum momentum transfer between a parton of energy E and one of $3T$. Setting $q_{\rm max} = \infty$ in ASW-SH is consistent with the change in integration variables performed in deriving Eq. (8). As will be shown below, this different choice of $q_{\rm max}$ has little effect on the jet energy loss.

It turns out that energy-momentum conservation is enforced in the cutoff of the $k_\perp$ integration. Naively one may expect that setting $k_{\rm max} = xE$, as is done in ASW-SH, would be sufficient. As one can see from any of the dN_g/dx figures, though, the single gluon spectrum does not naturally tend to 0 as x tends to 1 in this case; there is nonzero support for a single gluon to emerge with energy larger than that initially held by the parent parton. Not only does this large x behavior violate energy conservation, but it also violates the eikonal approximation (which assumes that the parent parton continues on a nearly straight-line path and gluons are radiated in the forward direction). WHDG enforces the assumed eikonality ($p^+ \gg p^-$ and $k^+ \gg k^-$, where p is the final momentum of the parent parton—see Fig. 1) by cutting off the $k_\perp$ integration at approximately $p^+ = p^-$ and $k^+ = k^-$ with $k_{\rm max} = 2x(1-x)E$. This leads, as one can see in the comparison plots Fig. 8 and on, to a single gluon spectrum that truly has no support for $x > 1$, consistent with energy conservation.

The integral of dN_g/dx over x gives the average number of emitted gluons,

$$\langle N_g \rangle = \int dx \frac{dN_g}{dx}. \tag{11}$$

The WHDG gluon spectrum with $k_{\rm max} = 2x(1-x)E$ has no support for $x > 1$, and the upper limit of integration for Eq. (11) is therefore $x = 1$. The ASW spectrum does have support for $x > 1$, and ASW-SH takes the

upper limit of integration to be $x = \infty$. The expressions for dN_g/dx above are inclusive expressions; there is no requirement that only one gluon be emitted. Multiple radiated gluons have so far been treated by assuming independent emissions. A Poisson distribution whose mean is $\langle N_g \rangle$ controls the number of emitted gluons, and the probability distribution of fractional momentum loss ϵ, $P(\epsilon)$, where the final momentum of the parent parton is related to the initial momentum by $p_\perp^f = (1-\epsilon)p_\perp^i$, is found by performing convolutions over x.

As will be seen more explicitly below the independent emission assumption in the Poisson convolution, which in part assumes that all the radiated gluons come from a parent parton of energy E, violates energy conservation. There are a number of options for dealing with this probability overflow but the two most common are to "reweigh" and to "truncate" [17]. Reweighing evenly redistributes the excess probability over the distribution for $\epsilon < 1$:

$$P_{\text{reweighed}}(\epsilon) = \frac{P_{\text{original}}(\epsilon)}{1 - \int_1^\infty d\epsilon' P_{\text{original}}(\epsilon')}\theta(\epsilon - 1). \tag{12}$$

Truncating places all the excess probability into a delta function centered at $\epsilon = 1$:

$$P_{\text{shovel}} = P_{\text{original}}(\epsilon)\theta(\epsilon - 1) + \delta(\epsilon - 1)\int_1^\infty d\epsilon' P_{\text{original}}(\epsilon'). \tag{13}$$

It was shown in [18] that relative branching, a method that is an improvement over both reweighing and truncation, produces results closely resembling truncation. In addition to being unphysical, redistributing the excess probability evenly gives excess weight to the low-ϵ probabilities which—due to the steeply falling spectrum in calculations for, e.g. R_{AA}—will disproportionately affect the results. In this note we will only employ the truncation method.

In the ASW-SH formalism, the convolution is performed over the gluon energy spectrum $dI/d\omega$ to produce a distribution of jet energy loss ΔE. The Laplace transform and its properties are exploited to evaluate the convolution; the sum is calculated in a single step as part of the transform and the inverse transform directly gives $P(\Delta E)$, which can be re-cast as $P(\epsilon)$. Since the dN_g/dx spectrum for ASW-SH does not go to zero as $x \to 1$ we expect the nonzero support for $\epsilon > 1$ in its $P(\epsilon)$ convolution to be larger than for WHDG.

In the WHDG approach the Poisson convolution is performed iteratively:

$$P(\epsilon) = \sum_n P_n(\epsilon), \tag{14}$$

where

$$\begin{aligned} P_0(\epsilon) &= e^{-\langle N_g\rangle}\delta(\epsilon) \\ &= P^0\delta(\epsilon) \end{aligned} \tag{15}$$

$$\begin{aligned} P_1(\epsilon) &= e^{-\langle N_g\rangle}\frac{dN_g}{dx}(\epsilon)\theta(1-\epsilon) + P_1^1\delta(\epsilon-1) \\ &= \tilde{P}_1(\epsilon) + P_1^1\delta(\epsilon-1) \end{aligned}$$

$$\vdots \tag{16}$$

$$\begin{aligned} P_n(\epsilon) &= \frac{1}{n}\int_0^1 dx\tilde{P}_{n-1}(x)\tilde{P}_1(\epsilon-x)\theta(1-\epsilon) + P_n^1\delta(\epsilon-1) \\ &= \tilde{P}_n(\epsilon) + P_n^1\delta(\epsilon-1), \end{aligned}$$

and the probability overflow is found from the normalization condition

$$P_n^1 = \frac{e^{-\langle N_g\rangle}\langle N_g\rangle^n}{n!} - \int_0^1 d\epsilon\tilde{P}_n(\epsilon). \tag{17}$$

While $P_{n\neq 1}^1 \neq 0$ in general note that with the WHDG $k_{\max} = 2x(1-x)E$ the single inclusive distribution has no support for $x > 1$, and $P_1^1 = 0$ by construction. Nevertheless we have explicitly included the term here for comparison to the ASW-SH results whose single inclusive spectrum is nonzero for $x > 1$ (and therefore $P_1^1 \neq 0$).

With these conventions Eq. (14) becomes

$$\begin{aligned} P(\epsilon) &= P^0\delta(\epsilon) + \sum_{n=1}\tilde{P}_n(\epsilon) + \sum_{n=1}P_n^1\delta(\epsilon-1) \\ &= P^0\delta(\epsilon) + \tilde{P}(\epsilon) + P^1\delta(\epsilon-1). \end{aligned} \tag{18}$$

We will denote the three contributions to the probability of energy loss $P(\epsilon)$ direct, continuous, and overflow corresponding to P^0, $\tilde{P}(\epsilon)$, and P^1, respectively; the direct and overflow parts will be called the discrete part of the probability distribution. In principle, the upper limit of the sums over n is $n_{max} = \infty$, but the Possion probability $P(N_g)$ naturally cuts off contributions from $n \gg \langle N_g\rangle$. In practice the WHDG calculations truncate the sum once the change in norm of $P(\epsilon)$ is guaranteed to be below some small, predetermined value.

3 Analysis Technique

To evaluate the origin of differences between the WHDG and ASW leading order opacity results, we have modified the WHDG dN_g/dx formula to

explicitly match the ASW form. Specifically this means

- Set the thermal gluon mass to 0.
- Set the thermal quark mass to 0.
- Use $k_{\max} = xE_{\rm jet}$.
- Use the ASW scattering center distribution, Eq. (3).
- Fix $L/\lambda = 1$.
- Use $q_{\max} = \infty$.
- Use $\alpha_s = 1/3$.

We call this configuration of WHDG *WHDG-ASWExact* and will show below that it reproduces the ASW-SH results to within the numerical precision of the calculations. We will then undo the changes to the WHDG formula one step at a time to show the evolution back to the original WHDG results. Figs. 3-10 visualize this unfolding of effects: black curves represent the ASW-SH output, red curves the current WHDG iteration, and blue curves the WHDG iteration from the previous figure (included to make the step-by-step differences more apparent). Table 1 quantifies the differences between configurations of the calculation by providing the values of: the average number of emitted gluons, $\langle N_g \rangle$; the average gluon x, $\langle x \rangle$; the direct term in $P(\epsilon)$, P^0; the overflow term P^1; and the average fractional energy loss $\langle \epsilon \rangle$.

For all of the studies in this note we will use parameters $T = 485$ MeV, $L = 2$ fm, and $E_{\rm jet} = 10$ GeV. WHDG takes $\mu = gT$, and we use this value as an input in the ASW-SH code. For $\alpha_s = 1/3$ this gives $\mu \simeq 0.99$ GeV, and $\alpha_s = 0.3$ yields $\mu \simeq 0.94$ GeV. For L/λ not fixed WHDG uses $\lambda = 1/\rho\sigma$ with $\sigma = 9\pi\alpha_s^2/2\mu^2$; for $\alpha_s = 0.3$ then $\lambda \simeq 0.62$ fm.

To perform these comparisons we have used three different methods to evaluate the single gluon spectrum and $P(\epsilon)$:

1. A C++ interface to the public ASW quenching weights code.
2. WHDG calculations including modifications described above using Mathematica performed by WAH.
3. Independent numerical calculations of the single gluon spectrum and $P(\epsilon)$ implemented in C++ code by BAC with all possible combinations of modifications appearing in the above list.

Since the ASW quenching weights code does not provide the single gluon distribution, the dN_g/dx results shown below for the ASW-SH calculation are obtained using BAC's code evaluating exactly the integral in Eq. (10). To evaluate the consistency between the new numerical calculations implemented by BAC and the original ASW quenching weights code, we show in Fig. 2, a comparison of the quark quenching weight, $P(\epsilon)$ for $L = 2$ fm, $\mu = 0.993$ GeV and using the ASW limits and phase factor in evaluating dN_g/dx. The agreement between the original ASW results and the new numerical results is good though not perfect. The continuous quenching weight matches exactly over the entire x range, but there is a 2% disagreement in the discrete quenching weight and factor of two difference between the (small) overflow terms. We note, however, that the Poisson convolution is performed differently by ASW and the numerical code which uses the iterative approach described above. The differences between the two calculations in the overflow region likely results from the different approaches used to evaluate the convolution.

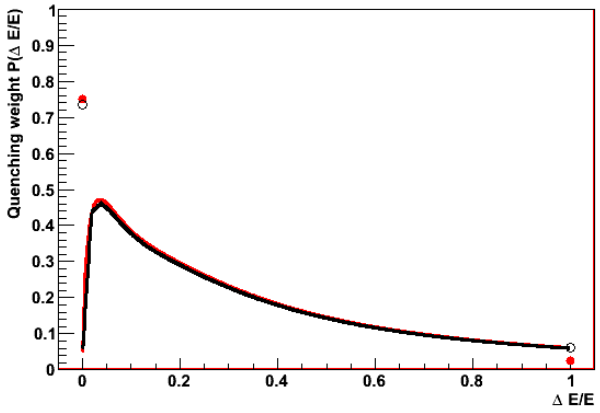

Figure 2: Comparison of ASW-SH (black) and new numerical code evaluation of quark quenching weight for $L = 2$ fm, $E = 20$ GeV, $\mu = 0.993$ GeV and using a configuration of the numerical code that matches the ASW integration limits and phase factor in evaluating dN_g/dx.

4 ASW-SH, WHDG Comparisons

The comparison of the ASW-SH and *WHDG-ASWExact* results for the gluon spectrum and quenching weights are given in Fig. 3. These results are obtained for $\alpha_s = 1/3$ in contrast with the remaining WHDG calculations performed for $\alpha_s = 0.3$. Aside from slight differences attributed to the discrete binning in the ASW-SH quenching weights code, the results are in good agreement. Table 1 shows values for total number of emitted gluons, average gluon x, and the discrete quenching weights for both calculations for all WHDG configurations including *WHDG-ASWExact*. The differences in these quantities are at the level of numerical precision.

Most of the WHDG calculations have historically been performed with $\alpha_s = 0.3$ instead of $\alpha_s = 1/3$. For fixed L/λ dN_g/dx is linear in α_s, and the effects of this change are expected to be modest. We show in Fig. 4 the results of changing to $\alpha_s = 0.3$ in the WHDG calculation and leaving all other aspects of the WHDG calculation the same as for *WHDG-ASWExact*. We call this configuration *WHDG-*α_s. As can be seen from the figure and from Table 1 the slight decrease in coupling constant produces an overall multiplicative reduction in the continuous quenching weight and a slight increase in the discrete weight at zero.

The expressions for the single gluon spectrum above require an integration over q the momentum transfer from the scattering center. the ASW-SH and WHDG calculations treat the upper limit on this integral, $q_{\max}$, differently. ASW-SH takes $q_{\max} = \infty$ while WHDG takes $q_{\max} = \sqrt{3\mu E}$. To evaluate the effect of this difference, we start from the *WHDG-*α_s and restore the WHDG value for $q_{\max}$. The results of this configuration, *WHDG-*$q_{\max}$, are shown in Fig. 5. As the results in the figure indicate, the difference resulting from the choice of $q_{\max}$ are barely visible.

As noted above, the first order in opacity result for the gluon spectrum is proportional to L/λ. The ASW-SH quenching weights calculation uses $L/\lambda = 1$. The above WHDG results have been obtained for $L/\lambda = 1$ to match the ASW-SH calculations. We show in Fig. 6 the result of restoring the the L/λ factor. The resulting configuration, *WHDG-*L/λ, is otherwise identical to *WHDG-*α_s. For the chosen parameters of the calculation, $T = 485$ MeV and $\alpha_s = 0.3$, the quark mean free path is $\lambda = 0.62$ yielding $L/\lambda = 3.2$. The gluon spectrum in the figure shows the approximately factor of three increase in magnitude due to the L/λ factor. The quenching weights show a corresponding decrease in the discrete weight at $\epsilon = 0$ and an increase in the scale of the continuous quenching weight. The increase in the number of emitted gluons also increases the overflow term in the quenching

weight so that roughly 20% of the probability distribution corresponds to $\epsilon > 1$.

The next feature of the original WHDG calculation that we return is the exponential distribution of scattering centers, accomplished by restoring the factor in the square bracket in Eq. (7); we label this change *WHDG-ExpPhase*. Since the exponential distribution weights the probability of scattering close to the production point more as compared to the theta distribution (even though the average distance is the same) we expect the destructive interference associated with the smaller x, more collinear gluons to increase. This is what we see in Fig. 7. The modification of the phase factor has a modest impact on the gluon spectrum with the largest effect near its peak at small x. The exponential phase reduces the overall number of gluons by $\approx 10\%$, but it also makes the gluon distribution flatter, increasing the relative yield in the unphysical region $x > 1$.

The next step in evolving back, configuration *WHDG-Kmax*, involves replacing $k_{\rm max} = \omega$ with $k_{\rm max} = 2x(1-x)E_{\rm jet}$. As discussed above, this change has the feature that it forces the single gluon spectrum to zero at $x = 1$; nevertheless the convolution for multiple gluon emissions still generates non-zero probability for $\epsilon > 1$. The additional factor of two is also worth noting as it opens up the phase space for gluon emission even in the region $x \ll 1$. We will return to investigate the impact of this factor of two below. The results of *WHDG-Kmax* compared to the ASW-SH quenching weights are shown in Fig. 8. The change in the upper limit of the $K_\perp$ integration produces a large increase in the number of emitted gluons and the continuous quenching weights at small x along with the expected truncation of the dN_g/dx at $x = 1$. This truncation of the gluon distribution at the kinematic limit substantially reduces the quenching weight at $x = 1$ compared to *WHDG-ExpPhase* even though the overall gluon yield increases by more than a factor of two.

The next step in restoring the original WHDG calculation is to reintroduce quark and gluon thermal masses. We first show results for non-zero quark mass (*WHDG-QuarkMass*) in Fig. 9. The non-zero quark masses produce negligible change in the gluon spectrum and quenching weights compared to the *WHDG-Kmax* calculations. However, calculations with non-zero gluon mass (*WHDG-Massive*) shown in Fig. 10 show a very different result. The gluon mass produces nearly a factor of three suppression of the radiated gluon spectrum at the peak while producing very little change in the spectrum for $x > 0.3$. Thus, the incorporation of the gluon mass hardens the spectrum while reducing the overall gluon yield by 40%.

	dN_g/dx		Convolution		
WHDG Config	$\langle N_g \rangle$	$\langle x_g \rangle$	P^0	P^1	$\langle \varepsilon \rangle$
ASW-SH	0.29	0.48	0.73	0.06	0.12
WHDG-ASWExact	0.31	0.50	0.74	0.08	0.14
WHDG-QMax	0.25	0.46	0.78	0.05	0.11
WHDG-Alphas	0.26	0.49	0.77	0.07	0.12
WHDG-LOverLambda	0.81	0.46	0.45	0.17	0.31
WHDG-ExpPhase	0.76	0.47	0.47	0.17	0.30
WHDG-Kmax	1.08	0.18	0.34	0.01	0.19
WHDG-QuarkMass	1.11	0.18	0.33	0.01	0.20
WHDG-ThermalMasses	0.74	0.24	0.48	0.01	0.17
ASW-2xE	0.61	0.33	0.55	0.05	0.35
ASW-ExpPhase	0.28	0.52	0.75	0.03	0.45
ASW-LOverLambda	1.03	0.48	0.36	0.19	0.58

Table 1: Table of quantities characterizing the results from the different WHDG configurations and the ASW-SH quenching weights. Those from the single inclusive distribution are defined as $\langle N_g \rangle = \int dx\, dN_g/dx$ and $\langle x_g \rangle = \int dx\, x\, dN_g/dx$. Those resulting from the convolution are the discrete, P^0, and continuous, P^1, parts of the $P(\epsilon)$ distribution—Eq. (15) and Eq. (18), respectively—and the average fractional energy loss, $\langle \epsilon \rangle = \int d\epsilon\, \epsilon\, P(\epsilon)$.

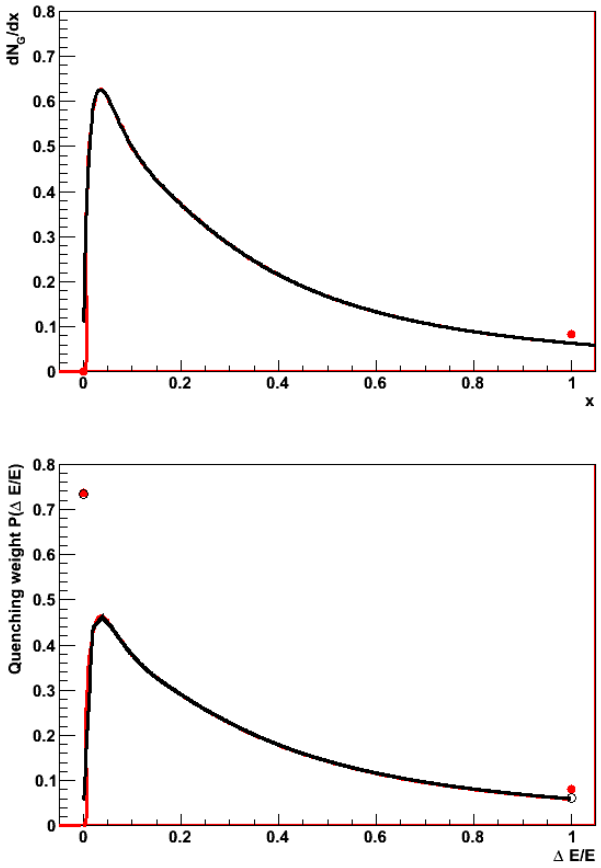

Figure 3: Comparison of ASW-SH (black) and *WHDG-ASWExact* (red) gluon spectra (top) and quenching weights (bottom). For the quenching weights, the solid curves show the continuous quenching weights while the open (solid) circles show the ASW-SH (WHDG) discrete quenching weights at $x = 0$ and $x = 1$

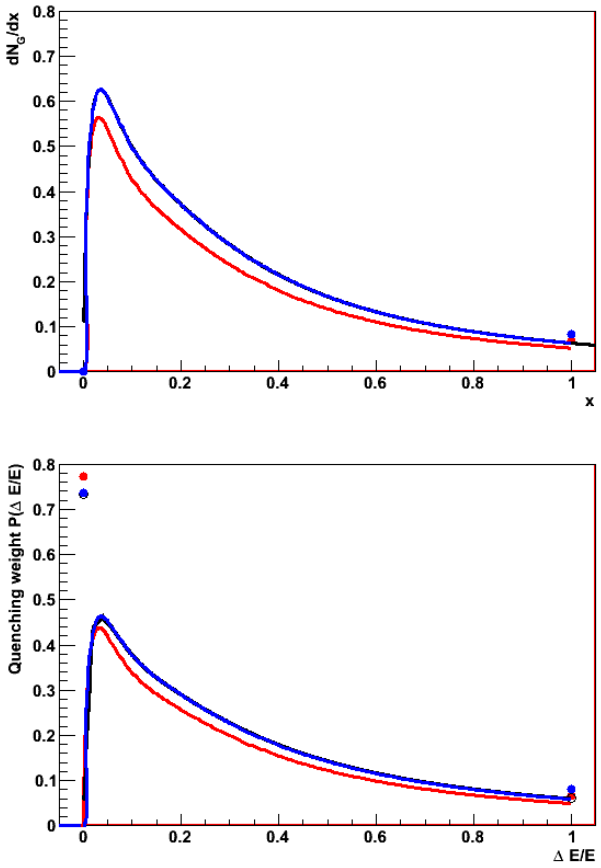

Figure 4: Comparison of ASW (black), *WHDG-α_s* (red), and *WHDG-ASWExact* (blue) gluon spectra (top) and quenching weights (bottom). For the quenching weights, the solid curves show the continuous quenching weights while the open (solid) circles show the ASW (WHDG) discrete quenching weights at $x = 0$ and $x = 1$

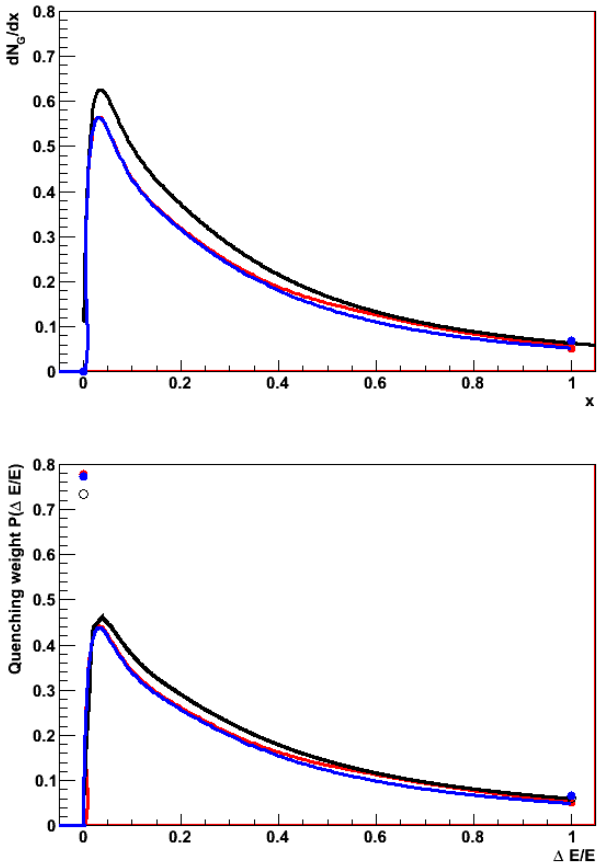

Figure 5: Comparison of ASW-SH (black), *WHDG*-$q_{\max}$ (red), and *WHDG*-α_s (blue) gluon spectra (top) and quenching weights (bottom). For the quenching weights, the solid curves show the continuous quenching weights while the open (solid) circles show the ASW-SH (WHDG) discrete quenching weights at $x = 0$ and $x = 1$

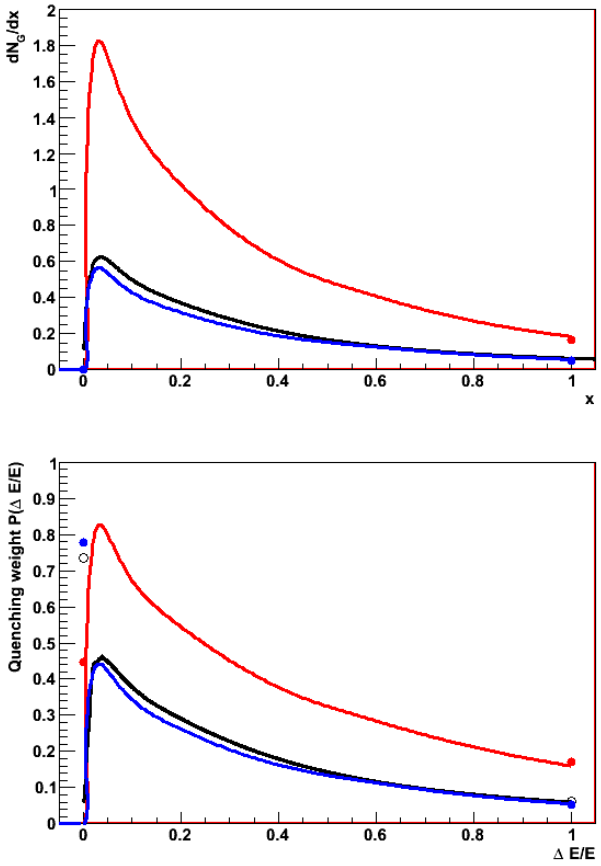

Figure 6: Comparison of ASW-SH (black), *WHDG*-L/λ (red), *WHDG*-$q_{\max}$ (blue) gluon spectra (top) and quenching weights (bottom). For the quenching weights, the solid curves show the continuous quenching weights while the open (solid) circles show the ASW-SH (WHDG) discrete quenching weights at $x = 0$ and $x = 1$

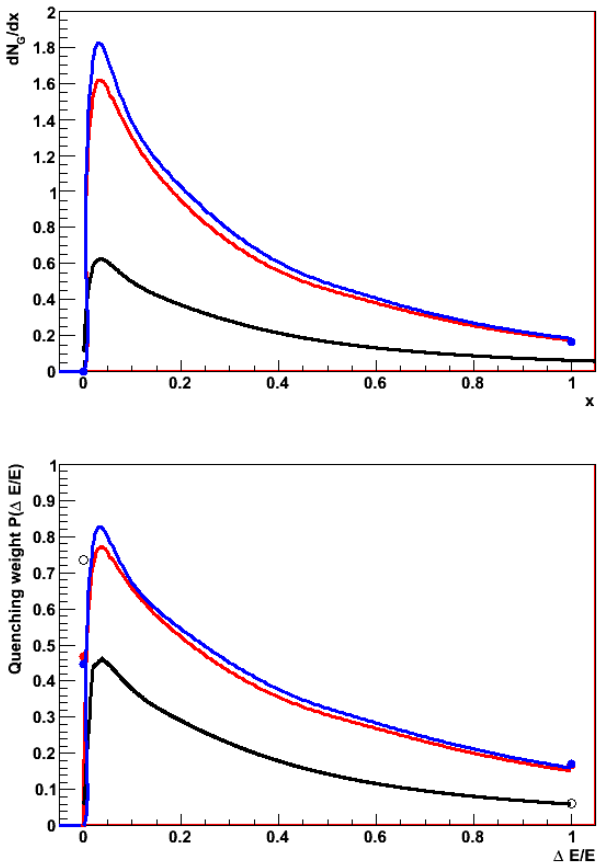

Figure 7: Comparison of ASW-SH (black), *WHDG-ExpPhase* (red), and *WHDG-L/λ* (blue) gluon spectrum (top) and quenching weights (bottom). For the quenching weights, the solid curves show the continuous quenching weights while the open (solid) circles show the ASW-SH (WHDG) discrete quenching weights at $x = 0$ and $x = 1$

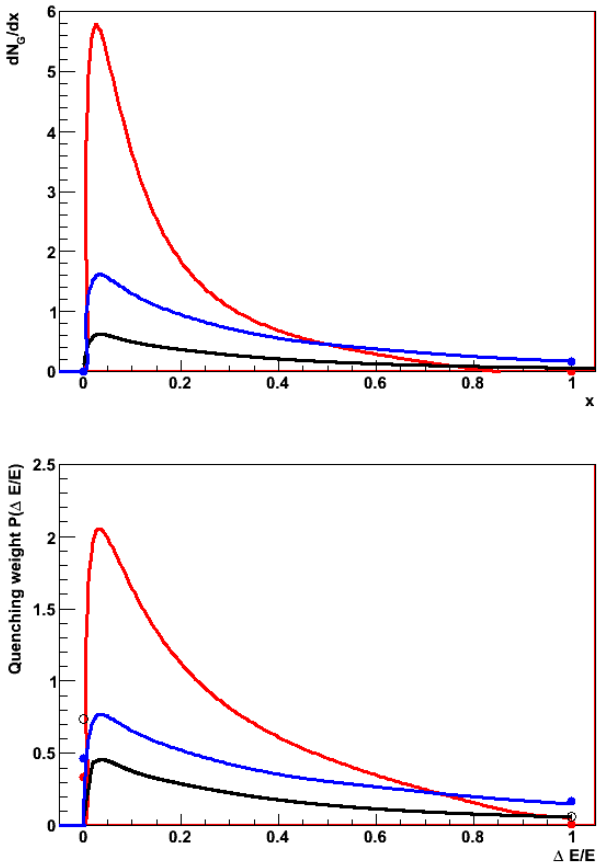

Figure 8: Comparison of ASW-SH (black), *WHDG-Kmax* (red), and *WHDG-ExpPhase* (blue) gluon spectra (top) and quenching weights (bottom). For the quenching weights, the solid curves show the continuous quenching weights while the open (solid) circles show the ASW-SH (WHDG) discrete quenching weights at $x = 0$ and $x = 1$

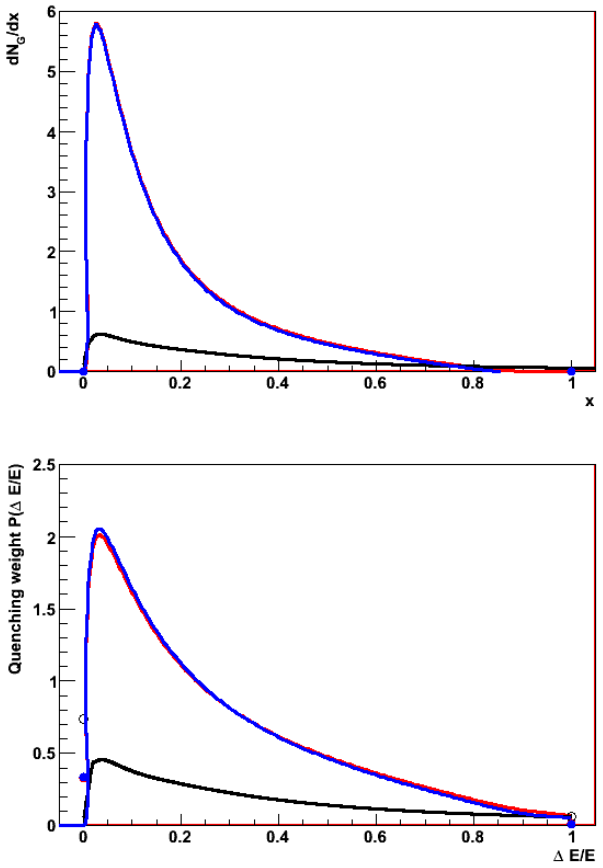

Figure 9: Comparison of ASW-SH (black), *WHDG-QuarkMass* (red), and *WHDG-Kmax* (blue) gluon spectra (top) and quenching weights (bottom). For the quenching weights, the solid curves show the continuous quenching weights while the open (solid) circles show the ASW-SH (WHDG) discrete quenching weights at $x = 0$ and $x = 1$

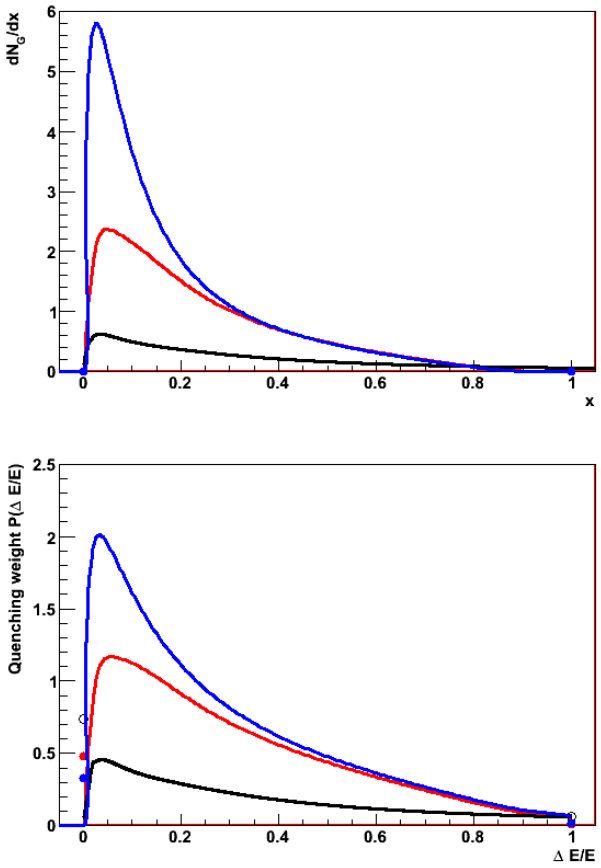

Figure 10: Comparison of ASW-SH (black), *WHDG-Orig* (red) gluon, and *WHDG-QuarkMass* (blue) spectra (top) and quenching weights (bottom). For the quenching weights, the solid curves show the continuous quenching weights while the open (solid) circles show the ASW-SH (WHDG) discrete quenching weights at $x = 0$ and $x = 1$

5 Further studies

The above analysis quantifies the numerical differences arising between ASW-SH quenching weight and WHDG implementations by starting from *WHDG-ASWExact* (WHDG altered to reproduce ASW-SH) and successively removing these modifications. However, a direct evaluation of the impact of the most significant changes in the calculation would also be helpful. To this end, we present here results using the numerical code by BAC of the modifications to the gluon spectrum and $P(\epsilon)$ resulting from changes to a single parameter or aspect of the calculation. In all cases, we start from the default ASW calculation with $L = 2$ GeV, $E_{\rm jet} = 20$ GeV, $\alpha_s = 1/3$ and $\mu = 0.993$ GeV.

We start by evaluating the impact of the factor of two in the WHDG $k_{\rm max}$ by comparing in Fig. 11 results for the default ASW calculation to those obtained with $k_{\rm max} = 2xE$. The figure shows that a factor of two change in the upper limit of the k integration produces a factor of ~ 4 change in the gluon spectrum at low x and a factor of ~ 3 increase in the continuous quenching weight at low ϵ. At large x and ϵ, respectively, the gluon spectrum and quenching weights have only modest sensitivity to this change in $k_{\rm max}$.

To directly evaluate the impact of the change in the phase factor in the q integral, we show in Fig. 12 a comparison between the default ASW calculation and the result obtained with the GLV/WHDG phase function. The gluon spectra from the two calculations differ significantly only at the peak of the gluon spectrum and then only by 20%. The change in the phase factor has little or no impact on the gluon spectrum or the quenching weight for x or ϵ larger than 0.1. Fig. 12 provides a refinement on the conclusions drawn from Fig. 7 where the calculations used a finite $q_{\rm max}$.

For completeness, we show in Fig. 13 a comparison between the default ASW calculation and one with a non-unity L/λ factor, where $\lambda \simeq 0.558$ fm corresponds to $\alpha = 1/3$ and $T = 485$ MeV. The resulting $L/\lambda \simeq 3.6$ factor simply multiplies the single gluon spectrum dN_g/dx; while $\langle N_g \rangle$ increases, $\langle x_g \rangle$ is unaffected (see Table 1). However this trivial change in normalization of the single gluon spectrum has a highly nontrivial result in $P(\epsilon)$: the Poisson convolution now weighs its individual P_n contributions differently. In particular as $\langle N_g \rangle \sim 1$ instead of $\ll 1$ the much broader P_2 term becomes significant, and the large x region of dN_g/dx becomes more important; we will explore this in more detail below. Quantitatively, the result is a factor of ~ 2 increase in the continuous quenching weight and a factor of ~ 2 decrease in the discrete quenching weight at $x = 0$. The increase in the amplitude

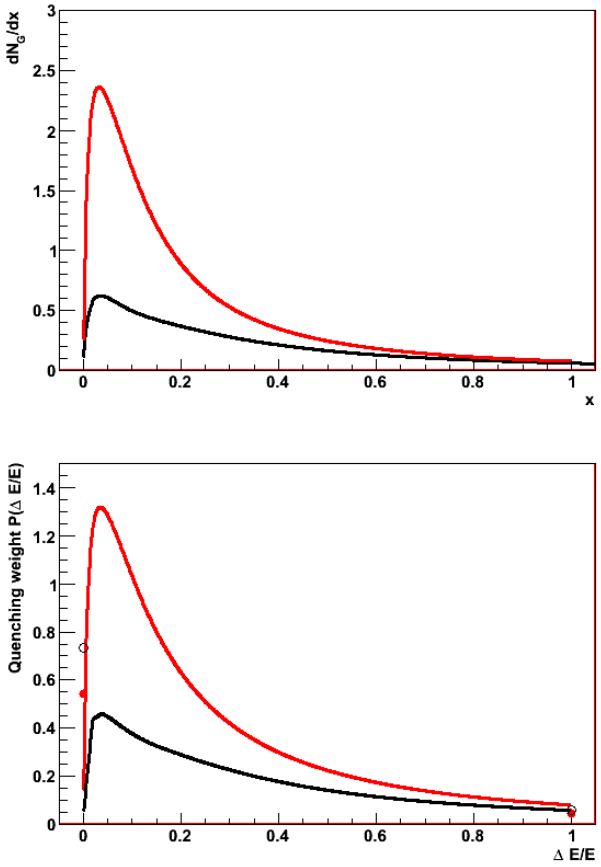

Figure 11: Comparison of gluon spectrum (top) and $P(\epsilon)$ (bottom) between default ASW calculation and a calculation with $k_{\max} = 2xE$ obtained using the numerical code by BAC.

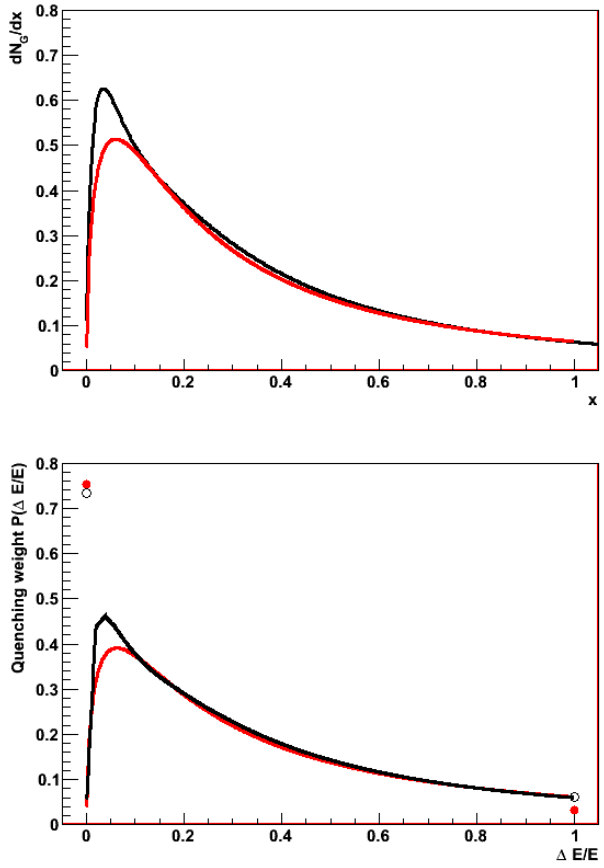

Figure 12: Comparison of gluon spectrum (top) and $P(\epsilon)$ (bottom) between default ASW calculation and a calculation using the GLV/WHDG phase function.

of the gluon spectrum exacerbates the violation of energy conservation in the convolution; as shown in Table 1, the overflow contribution P^1 increases by more than a factor of ~ 3. As will be shown below, the proportionately larger increase in P^1 compared to $P(\epsilon)$ at the peak is due to the multiple gluon convolution in the quenching weight calculation and the increase in the average number of emitted gluons resulting from the inclusion of the L/λ factor.

The derivation of the emission spectrum for both ASW and DGLV uses the soft gluon, or small x, approximation. This assumption is generally *a posteriori* justified by the high peaking of the spectrum for small values of x. However when $\langle N_g \rangle \gtrsim 1$ the Poisson approximation of multiple gluon emission, which convolves dN_g/dx with itself over all x, induces a sensitivity in $P(\epsilon)$ at large ϵ to the shape of the dN_g/dx spectrum at large x; recall from Eq. (17) that the P_n contributions are normalized to $\exp(-\langle N_g \rangle)\langle N_g \rangle^n/n!$, and hence P_n makes an important contribution to $P(\epsilon)$ for $n \sim \langle N_g \rangle$. In particular the sensitivity of the quenching weight calculation to large-x contributions increases if the amplitude of the gluon spectrum is increased, even if the shape of the spectrum is left unchanged. To see this quantitatively we show in Fig. 14 a breakout of the $n = 1$ and $n = 2$ contributions to the quenching weight compared to the complete quenmching weight for the default ASW calculation (with $\langle N_g \rangle \simeq 0.29$). For that calculation, the $n = 1$ term clearly dominates. The $n = 2$ contribution to the quenching weight, resulting from a single convolution of the single gluon spectrum, is both sufficiently broad and small in normalization that it only contributes in the region $\epsilon \gtrsim 0.15$, and at a small level.

Since the size of the $n = 2$ term and higher n terms in the Poisson convolution is determined by $\langle N_g \rangle$, if the single gluon spectrum is increased significantly, the contributions of the $n > 1$ terms to the quenching weight becomes more important. To illustrate this behavior, we show in Fig. 15 the contribution of the $n = 1$, $n = 2$, and $n = 3$ terms to the complete quenching weight for the ASW calculation incorporating the $L/\lambda \simeq 3.6$ factor shown in Fig. 13 (with $\langle N_g \rangle \simeq 1.04$). The $n = 2$ term contributes significantly to the quenching weight for $\epsilon > 0.2$ while the small $n = 3$ term contributes little and only in the region $\epsilon > 0.3$. Note that the severe broadening of the $n = 2$ and $n = 3$ terms in the Poisson convolution is largely due to the tail of the gluon dN/dx spectrum to large x, and we see quantitatively the importance of the large x region of dN_g/dx in determining the large ϵ behavior of the quenching weight $P(\epsilon)$.

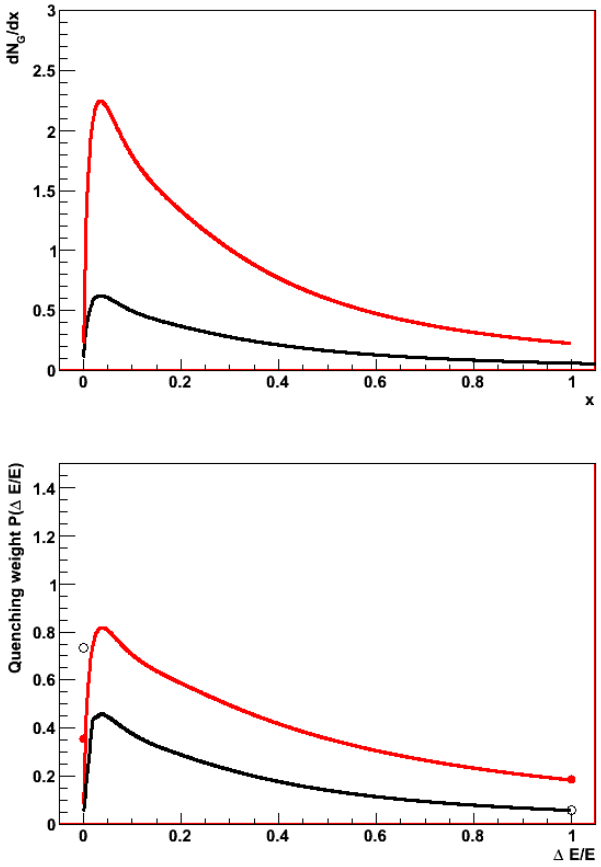

Figure 13: Comparison of gluon spectrum (top) and $P(\epsilon)$ (bottom) between default ASW calculation with $L/\lambda = 1$ and a calculation with $L/\lambda \simeq 3.6$ obtained using the numerical code by BAC.

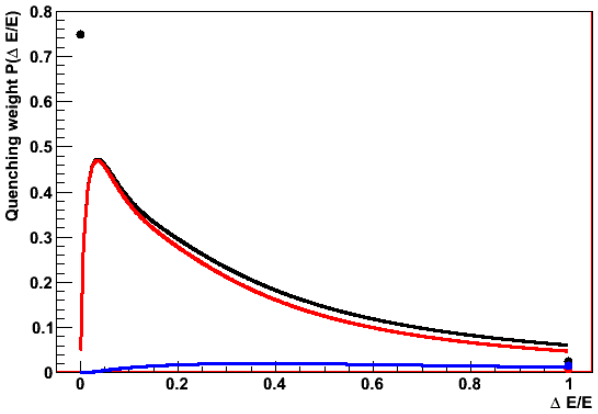

Figure 14: Breakout of the $n = 1$ (red) and $n = 2$ (blue) contributions to the complete quenching weight (black) for the default ASW calcualtion with $L/\lambda = 1$.

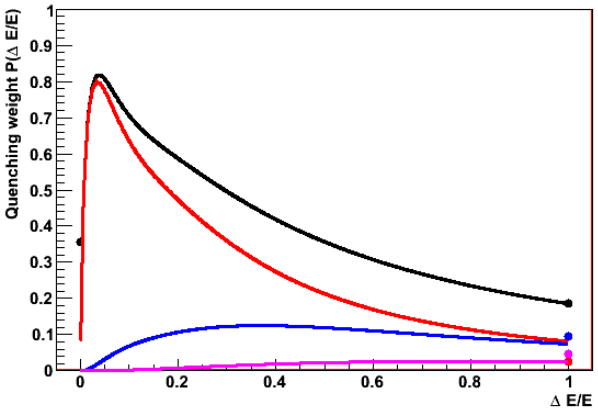

Figure 15: Breakout of the $n = 1$ (red), $n = 2$ (blue), and $n = 3$ (purple) contributions to the complete quenching weight (black) for the ASW calcualtion incorporating a real L/λ factor ($L/\lambda = 3.6$).

6 Conclusions

From the above analysis, there are three major differences between the ASW-SH calculations as implemented in the quenching weights code and the WHDG calculations that lead to significant modifications to the radiated gluon spectrum. These are

- The explicit choice of $L/\lambda = 1$ in ASW-SH quenching weights.
- The upper limit of the k integration, in particular the factor of 2 in the WHDG choice $2x(1-x)E$.
- The incorporation of the gluon mass in the WHDG calculations.

Despite the significant variation in form induced by the different scattering center distributions, the change produced a much smaller variation in the gluon spectrum than the three listed above. However, there may be an interaction between changes in the phase parameter and the choice of q_{max}; further investigation of this possibility is currently underway. Of the three sources of difference between the ASW-SH and WHDG calculations, the first was expected. The choice by ASW of a particular L/λ to best match their soft multiple scatter results is explicitly discussed in their paper. However, in the context of the TECHQM effort and the brick studies it is clear that fixing $L/\lambda = 1$ dramatically alters the results of the calculations for a given choice of μ, L, and $E_{\rm jet}$.

The magnitude of the modifications from the second and third items comes as a surprise. The discussions of the upper limit of the k integral have primarily focused on the $1-x$ factor. The physics implications of that term providing a cut-off of the gluon spectrum are clearly of interest. However, we conclude that the difference of the factor of between xE and $2x(1-x)E$ is of much greater significance and impact on the quenching. This change increases the gluon yield at the maximum of the spectrum by nearly a factor of three, though the increase in the total number of emitted gluons is more modest due to the decrease in gluon yield at large x. In this study the difference of the factor of two results from the implicit or explicit assumptions regarding the definition of x. In general, though, one would have hoped that the spectra would be insensitive to the exact value of the cutoffs, which are at best known up to some $\mathcal{O}(1)$ factor. At this point these large effects resulting from the imprecise knowledge of the kinematics and radiated gluon mass are a systematic theoretical uncertainty. Clearly reducing these uncertainties and resolving the difference in theoretical interpretation is a high priority.

References

[1] S. Wicks, W. Horowitz, M. Djordjevic, and M. Gyulassy, *Elastic, Inelastic, and Path Length Fluctuations in Jet Tomography*, Nucl. Phys. **A784**, 426 (2007) [arXiv:nucl-th/0512076]. 2

[2] C. A. Salgado and U. A. Wiedemann, *Calculating quenching weights*, Phys. Rev. **D68**, 014008 (2003) [arXiv:hep-ph/0302184]. 2, 5

[3] M. Djordjevic and M. Gyulassy, *Heavy quark radiative energy loss in QCD matter*, Nucl. Phys. **A733**, 265 (2004) [arXiv:nucl-th/0310076]. 2, 3, 4

[4] M. Gyulassy, P. Levai, and I. Vitev, *Jet quenching in thin quark-gluon plasmas. I: Formalism*, Nucl. Phys. **B571**, 197 (2000) [arXiv:hep-ph/9907461]. 2

[5] M. Gyulassy, P. Levai, and I. Vitev, *Non-Abelian energy loss at finite opacity*, Phys. Rev. Lett. **85**, 5535 (2000) [arXiv:nucl-th/0005032].

[6] M. Gyulassy, P. Levai, and I. Vitev, *Reaction operator approach to non-Abelian energy loss*, Nucl. Phys. **B594**, 371 (2001) [arXiv:nucl-th/0006010]. 2

[7] M. Gyulassy, P. Levai, and I. Vitev, *Jet tomography of Au + Au reactions including multi-gluon fluctuations*, Phys. Lett. **B538**, 282 (2002) [arXiv:nucl-th/0112071]. 2

[8] S. Wicks, *Up to and beyond ninth order in opacity: Radiative energy loss with GLV* (2008) [arXiv:0804.4704]. 2

[9] W. A. Horowitz, *0th Order Heavy Quark Photon Bremsstrahlung* (2008) [arXiv:0806.3092]. 4

[10] M. Djordjevic and M. Gyulassy, *The Ter-Mikayelian effect on QCD radiative energy loss*, Phys. Rev. **C68**, 034914 (2003) [arXiv:nucl-th/0305062]. 4

[11] U. A. Wiedemann, *Gluon radiation off hard quarks in a nuclear environment: Opacity expansion*, Nucl. Phys. **B588**, 303 (2000) [arXiv:hep-ph/0005129]. 5

[12] R. Baier, Y. L. Dokshitzer, A. H. Mueller, S. Peigne, and D. Schiff, *Radiative energy loss of high energy quarks and gluons in a finite-volume*

quark-gluon plasma, Nucl. Phys. **B483**, 291 (1997) [arXiv:hep-ph/9607355]. 5

[13] R. Baier, Y. L. Dokshitzer, A. H. Mueller, S. Peigne, and D. Schiff, *Radiative energy loss and p(T)-broadening of high energy partons in nuclei*, Nucl. Phys. **B484**, 265 (1997) [arXiv:hep-ph/9608322].

[14] R. Baier, Y. L. Dokshitzer, A. H. Mueller, and D. Schiff, *Medium-induced radiative energy loss: Equivalence between the BDMPS and Zakharov formalisms*, Nucl. Phys. **B531**, 403 (1998) [arXiv:hep-ph/9804212].

[15] B. G. Zakharov, *Light-cone path integral approach to the Landau-Pomeranchuk-Migdal effect*, Phys. Atom. Nucl. **61**, 838 (1998) [arXiv:hep-ph/9807540]. 5

[16] N. Armesto, C. A. Salgado, and U. A. Wiedemann, *Medium-induced gluon radiation off massive quarks fills the dead cone*, Phys. Rev. **D69**, 114003 (2004) [arXiv:hep-ph/0312106]. 5

[17] A. Dainese, C. Loizides, and G. Paic, *Leading-particle suppression in high energy nucleus nucleus collisions*, Eur. Phys. J. **C38**, 461 (2005) [arXiv:hep-ph/0406201]. 7

[18] S. Wicks, *Fluctuations with small numbers: Developing the perturbative paradigm for jet physics in the QGP at RHIC and LHC*, Ph.D. thesis, Columbia University (2008). 7